IIETA International Information and Engineering Technology Association
Advancing the World of Information and Engineering

Traitement du Signal
Vol. 40, No. 3, June, 2023, pp. 1075-1082
Journal homepage: http://iieta.org/journals/ts

Enhancing the Resolution of Historical Ottoman Texts Using Deep Learning-Based Super-Resolution Techniques

Hakan Temiz

Department of Computer Engineering, Artvin Çoruh University, Artvin 08000, Turkey

Corresponding Author Email: htemiz@artvin.edu.tr

https://doi.org/10.18280/ts.400323

Received: 17 December 2022
Accepted: 12 March 2023

Keywords:
historical text image, super resolution, Ottoman, archive, document, deep learning

ABSTRACT

The Ottoman Empire's extensive archives hold valuable insights into centuries of history, necessitating the preservation and transfer of this rich heritage to future generations. To facilitate access and analysis, numerous digitization efforts have been undertaken to transform these valuable resources into digital formats. The quality of digitized documents directly impacts the success of tasks such as text search, analysis, and character recognition. This study aims to enhance the resolution and overall image quality of Ottoman archive text images using four deep learning-based super-resolution (SR) algorithms: VDSR, SRCNN, DECUSR, and RED-Net. The performance of these algorithms was assessed using SSIM, PSNR, SCC, and VIF image quality measures (IQMs) and evaluated in terms of human visual system perception. All SR algorithms achieved promising IQM scores and a significant improvement in image quality. Experimental results demonstrate the potential of deep learning-based SR techniques in enhancing the resolution of historical Ottoman text images, paving the way for more accurate character recognition, text processing, and analysis of archival documents.

1. INTRODUCTION

The super-resolution (SR) of historical document images has become a crucial prerequisite for designing and developing robust document processing and analysis systems. Text image super-resolution (TISR) plays a significant role in this context, as it aims to enhance the resolution and quality of these images. This is particularly important for low-quality historical documents, which often suffer from various negative deformations, wear, and deterioration. Factors such as scanning device properties and environmental lighting levels directly affect the resolution and quality of historical documents, making it challenging to read, process, and analyze their content. Undoubtedly, improving the resolution of these documents will facilitate the processing and analysis of historical text images.

The Ottoman Empire has left behind an enormous archival legacy, both in size and richness. However, the approximately 150 million documents in the Ottoman archive today represent only 25-30% of the empire's main archive [1]. Ottoman archives encompass various forms, including books, documents, magazines, newspapers, maps, postcards, manuscripts, paintings, photographs, and others. Numerous studies have focused on transferring Ottoman archive documents to digital media. A significant portion of these studies addresses character recognition, text search, automatic translation, and other related tasks. Image processing factors, such as image resolution, play a crucial role when converting Ottoman archive documents to digital images. The resolution of an image is one of the factors that most significantly affect image quality.

This study implements an SR application on Ottoman text images to enhance their overall quality and resolution. In this context, four different deep learning (DL) models, which have demonstrated success in other image types—such as daily images and medical images—have been utilized. These models were trained to magnify text images by factors of 2, 3, and 4, and their performance was measured using four different image quality metrics (IQM). Models' performances were also evaluated in terms of the human visual system. Studies have shown that the resolution and image quality of Ottoman archive text images can be efficiently improved. TISR applied to Ottoman archives will enable more successful optical character recognition, text analysis, text search, and image analysis tasks. To the best of our knowledge, this is the first study in which SR was implemented to improve the resolution of Ottoman archive documents.

2. LITERATURE

Super-resolution is an algorithmic solution that enhances resolution by leveraging image-specific a priori knowledge. It is a widely researched and applied problem in various imaging modalities, including daily photographs, aerial imaging, and medical imaging. An SR effort aims to produce finer details not present in the observed low-resolution (LR) version of high-resolution (HR) images while enlarging it by a scale factor.

Let x be desired HR image—e.g., sampled above Nyquist sampling rate from a continuous scene—, and y be LR image(s) of x, where can be obtained by:

$$y(i,j) = \mathfrak{D}(\mathfrak{B}(\mathfrak{M}(x))) + \mathfrak{n}(i,j) \quad (1)$$

where, y and x represent LR and HR images, respectively.

$\mathfrak{M}, \mathfrak{B}$ and $\mathfrak{D}$ are the functions of warping, blurring, downsampling operations, respectively. η is the term for an additive noise. According to the study [1], SR poses an inverse problem that HR images can be predicted from their LR counterparts.

In the past decades, algorithms have aimed to recover the relations between LR and HR images by exploiting various learning algorithms [2-5]. More recent approaches, such as example-based a priori learning, have involved deep learning (DL) algorithms with specific architectures, including convolutional neural networks (CNN) [6-8], AutoEncoders [9-11], generative adversarial networks (GAN) [12-15], and others. Since the application of SR in other research fields is beyond the scope of this study, interested researchers may refer to survey articles [16, 17].

Although not as common as in other image types (optical, medical, aerial, etc.), SR has also been applied to text document images to enhance the performance of systems for processing and analyzing such images. Various studies have contributed to this field, introducing new techniques and approaches to TISR [18-24]. Additionally, competitions have been established to encourage research in the TISR domain, such as the text image SR competition by Peyrard et al. [25].

Some research studies have aimed to improve the quality of text documents in the form of images, focusing on techniques other than TISR [26-29]. However, these efforts do not involve the implementation of TISR and are thus beyond the scope of this study.

Through diligent literature surveys, no study has been found that applied TISR to Ottoman archive documents. In this context, this study is the first of its kind. Furthermore, most studies applied their techniques to relatively small-sized image documents or fragments of documents. In contrast, this work required processing large-sized image documents, as they were in the form of large-size paper, newspaper, or book. Additionally, most studies utilized text images converted to binary images before processing. On the contrary, this study introduced archive text documents to the experiment as they were obtained during the scanning process.

3. MATERIALS AND METHODS

To implement SR on Ottoman archive documents, four different models were used: VDSR [7], SRCNN [6], DECUSR [8] and RED-Net [9]. Since the original architecture of some of these models–to be discussed in the following sections–was not designed to process 3-channel images, they were modified to process 3-channel images. The same data set as in the study [30] were used in the experiments. The dataset was constituted with the images collected from www.wikilala.com [31], where many historical documents and other materials are made available to its subscribers. This website, among other services it provides, also allows text search in historical Ottoman documents. The following sub sections present the details of the experiments such as dataset, models, training, test and results. Let us start with the dataset.

3.1 Dataset

There have been several serious digital archive transformation and collection studies carried out in order to unearth this enormously rich content and transfer it to future generations. Some of these were initiated by the state, while others were initiated by public institutions and private enterprises. Very few of them are as follows: Wikilala [31], Muteferriqa [32], Department of State Archives of Republic of Turkiye [33].

In this study, text images were collected from the Wikilala dataset. Total of 1166 historical text images were taken from the dataset, and were randomly and proportionally separated for training, testing and validation. Of them, 100 images are reserved for validation and another 100 for testing. The remaining 966 images were used for the training purposes. The web site serves images of the documents within pdf files consisting single or multi-page depending on the content. In essence, the images in the pdf files are of color scanned jpg files. The embedded jpg images were extracted from the pdf files with a program developed for this purpose.

As with all historical documents, unfavorable visual degradations, various shades and impurities were pervasively observed on these documents as well since they have been subjected to aging, wear, contamination, mouse droppings and peeing, etc. The text on the back pages of some scanned documents is also vaguely visible on the front page. Most of the images are books, notebooks, etc., which consist of manuscripts. Although the majority are handwritten documents, there are also printed documents such as newspaper pages. Some images are of poor visual quality due to insufficient lighting, contrast saturation, or scan sharpness. However, images are generally scanned at quite large sizes. The size of some images (width and height) reaches 4-5 thousand pixels of resolution. Some example images of the data set are given in Figure 1.

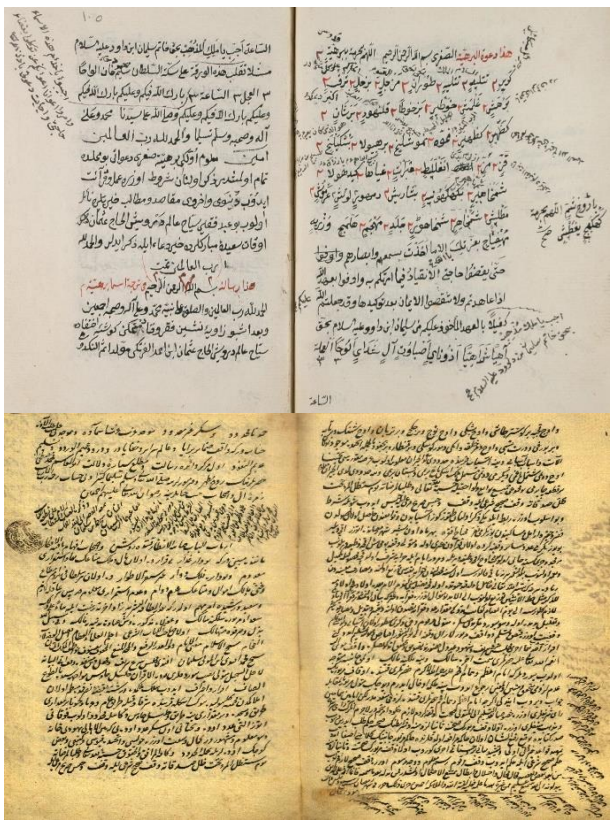

Figure 1. Two examples of Ottoman archive text images

3.2 Models and training

This section discusses the details of the models, given in alphabetical order, and implementation details of the training.

3.2.1 DECUSR

DECUSR was originally designed to process single-channel B-mode ultrasound images. Therefore, the network has been modified to process 3-channel images by inclusion of additional two filters in the last layer. The batch size value is 256. The initial learning rate was set to 1E-4 and programmatically halved when there is no improvement in its performance for successive 10 epochs. The dimensions of the input image fragments were determined in a similar way to the original. Namely, 16x16 pixel image pieces with 10 pixel interval, 11x11 pixel image segments with 7 pixel interval and 8x8 image segments with 4 pixel interval were taken from the training images for 2, 3, and 4 scale factors, respectively. The 'He Normal' method was used to initialize the layer weights. A series of studies were carried out to find the most successful parameter set of the model. These efforts were described in detail in the Ablation Study section.

3.2.2 SRCNN

The SRCNN model is originally designed to process the Y-channel of the YCbCr color space, which can be considered a single-channel image. Two additional filters were added to the last layer of the model, as applied to DECUSR, to make it suitable for processing 3-channel RGB images. Except for the channel increase in the last layer, the architecture of the network is exactly the same as the original. This model, which originally had around 8 thousand parameters, turned into a structure with 20,099 parameters after the channel adjustment.

The Learning rate is a hyper-parameter value that determines how much the layer weights will be updated in response to the error between the estimation of the model and the expected output during training of a model. In most studies, it has been seen that taking an initial value between 1E-3 and 1E-4 directly contributes to the rapid and successful learning of the model. Hence, the initial learning rate is taken as 1E-3. The Batchsize value is taken as 512. The model was trained with 33x33 pixel image patches taken at 11 pixel intervals from the training images, in line with the original article. The model's weights were initialized with the Glorot Uniform method.

3.2.3 VDSR

VDSR was also trained to enlarge images by 2x, 3x and 4x scales. The training was carried out for a maximum of 25 epochs. Adam optimizer was chosen as the optimizing algorithm. The initial learning rate was set to 1E-4 and halved when its performance has not increased for successive 15 epochs. The activation function was ReLU. The total number of parameters of the network is 668,227. The network was trained with image patches with 41x41 pixels in such a way that they do not overlap each other–taking each one 41 pixel apart. Batchsize was 256. The weights of the model were initialized with the 'He Normal' method.

When the training graphs are examined, though the training curve of VDSR for 2x magnification offers a relatively steady course, the validation curve followed a highly fluctuating course. As can be seen from the figure, the training was automatically terminated by the early stopping procedure at the 16th epoch due to the lack of improvement in the performance. However, the both training and validation curves of the other scales–3x and 4x–follow a relatively better smooth course. So, as happened in this experiment, some training processes may not converge nor be consistent in some cases. The preliminaries of this model was presented in the conference paper [30]. More details for the implementation and results can be found in this paper.

3.2.4 RED-Net

RED-Net is a relatively large-parameter model with encoder-decoder architecture. The first part of the algorithm operates as the encoder and the second part as the decoder. The output of the layers in the encoder section is given symmetrically in the decoder section with a shortcut link (skip connections) to the layers in the same symmetrical order. The RED30 model in the original study was used in our study. 64 filters of 3x3 kernels were used in the layers. Only the last layer has as many filters as the number of color channels of the rendered image. In this study, the same way as in the original, Adam optimizer was used and the initial learning rate was taken as 1E-4.

3.2.5 Common training details

In the trainings, the images were normalized by dividing by the maximum intensity value (255.0) before being fed to the networks. The bicubic interpolation method was used for the downsampling process. The mean-squared-error (MSE), whose formula is given in the following sections, was used as the penalty function. The same seed value was used in all studies to ensure reproducibility. Developments and all experiments were performed with the DeepSR [34] framework, which provides an integrated environment for all processes of the SR task—design, training, test, visualization, etc. The Tensorflow was chosen as the backend. All training, testing and validation processes were carried out on a computer with NVIDIA GeForce 2080Ti GPU. Table 1 provides some information about the models and trainings.

The training graphs of the models in PSNR measure are given in Figure 2. In the figures, the red, green, blue and magenta lines belong to DECUSR, SRCNN, VDSR and RED-Net, respectively. While the continuous lines show the training performance of the networks, the dashed lines indicate validation performance. Each column shows the training graph performed for the scales 2, 3 and 4—from left to right, respectively.

Table 1. The number of parameters and training times of the algorithms

Models	Parameters	Training Time (hours)		
		Scale-2	Scale-3	Scale-4
DECUSR	40,995	27.839	22.790	21.822
SRCNN	20,099	40.234	42.607	41.801
VDSR	668,227	26.303	40.605	40.147
RED-Net	1,037,507	90.047	89.099	91.0284

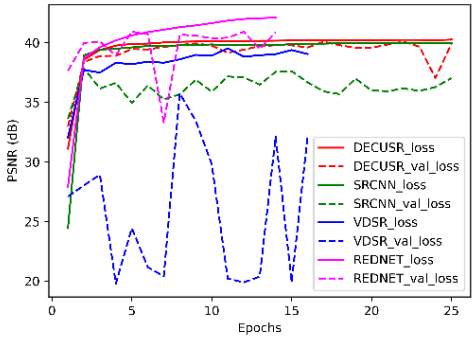

2x Scale

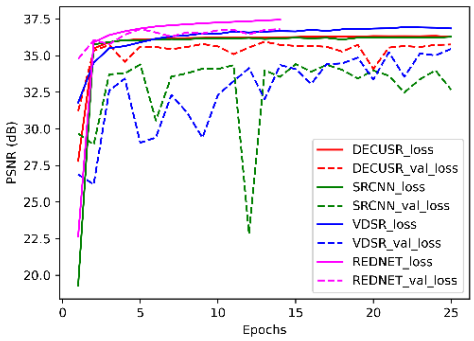

3x Scale

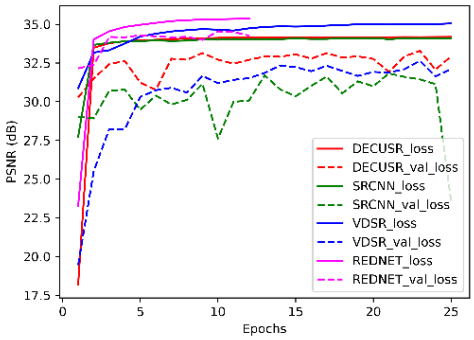

4x Scale

Figure 2. Training performances of the four models in PSNR

Because its performance did not improve for several epochs when training it for the 2x scale magnification, the training procedure of VDSR was terminated in the 16th epoch by early-stopping procedure. In addition, it can also easily be observed that it exhibits a rather fluctuating performance for this scale factor. Although the training graph of SRCNN is very close to the graph of DECUSR, it constantly remained below. The training and validation curves of RED-Net are generally above the other models. However, its training lasted around 14th epoch due to no improvement in the validation procedure for certain epochs, as happened to VDSR for 2x scale factor. This mechanism was set to prevent the overfitting. Although the training curve of VDSR is above the other two for the scales 2 and 4, its validation curves notably laid below them, with some exceptions where SRCNN's scores remain low. This may actually be a sign that it does not learn very well and is prone to overfit. Nevertheless, for the scale 3, both curves of VDSR are dramatically below the others. While the training curve of SRCNN is almost at the same level as the other models, the validation curve occurs at significantly lower levels. In addition, its validation curve is very fluctuating as well, which may be an indication of its instability in learning. DECUSR showed very stable and smooth-increasing training and validation curves until the end of the training. This should be a sign that the algorithm has a high ability to learn the transformation function from LR text image to HR text image.

3.3 Test

The performances of the algorithms were quantitatively evaluated by the following image quality metrics (IQM): Peak Signal to Noise Ratio (PSNR), Structural Similarity Index (SSIM) [35], Spatial Correlation Coefficient (SCC) [36] and Visual Information Fidelity (VIF) [37]. PSNR and SSIM are discussed in more detail in the following sections as they are more common IQMs.

Peak Signal to Noise Ratio (PSNR)

PSNR is a measure of the ratio of the maximum possible power of a signal to the power of noise affecting its representation fidelity. In short, it is the ratio of the maximum intensity value to the MSE—whose definition is given in (2)—between two images in logarithmic decibel (dB) scale. In image processing, it measures the discrepancy between reference and predicted image, and its value may range between 30 dB and 50 dB for 8-bit data [38]. The higher value of PSNR, the higher image quality.

The formal definition of PSNR is given in (3). Let us denote y and $\hat{y}$ respectively the reference and predicted image. MSE measures the distance between the images y and $\hat{y}$. It is defined as follows:

$$\mathrm{MSE} = \frac{1}{\mathrm{PR}} \sum_{i=1}^{P} \sum_{j=1}^{R} \|y(i,j) - \hat{y}(i,j)\|^2 \tag{2}$$

where, P and R denote the number of pixels in the height and width, respectively. PSNR is then computed as follows:

$$\mathrm{PSNR} = 20\log_{10}\left(\frac{L}{\sqrt{\mathrm{MSE}}}\right) \tag{3}$$

where, L is the maximum intensity value, which is 255.0 in our case (for 8-bit images).

Structural Similarity Index (SSIM)

SSIM measures perceptual quality of images with the similarity between two images—predicted and reference—in terms of three criteria: luminance, contrast, and structure. It incorporates some kind of gradient similarity functions to measure similarity, or in other saying, dissimilarity. The perceptual quality of an image is measured from three aspects: luminance, contrast, and structure. The product of above-mentioned three criteria computes the similarity score. SSIM considers the interdependencies of pixels in luminance, contrast, and structural terms. For given images y and $\hat{y}$, it is defined as follows:

$$\mathrm{SSIM}(y,\hat{y}) = \frac{(2\mu_y\mu_{\hat{y}} + c_1)(2\sigma_{y\hat{y}} + c)}{(\mu_y^2 + \mu_{\hat{y}}^2 + c_1)(\sigma_y^2 + \sigma_{\hat{y}}^2 + c_2)} \tag{4}$$

where, μ and σ are terms of the mean and variance of the corresponding image, and $\sigma_{y\hat{y}}$ is the covariance between both images. The coefficients c_1 and c_2 are calculated as follows:

$$c_1 = (k_1 L)^2 \tag{5}$$

$$c_2 = (k_2 L)^2 \tag{6}$$

The maximum density L is 255.0 for 8-bit images, and the default values of k_1 and k_2 are 0.01 and 0.03, respectively. SSIM is in the range of [0,1]. The values of 1.0 and 0.0 indicate the highest and poorest image quality, respectively.

SCC is measure of the correlation between two images by dividing their covariance by the product of their standard deviations.

VIF is a statistics model that measures the image deformations such as blur, additional noise, and local or general contrast changes, and takes into account the information theoretical setting of the human visual system.

In addition to the quantitative evaluation, qualitative evaluations were made in terms of the human visual system by examining some excerpts from the output text images of the algorithms. They are given in the next section.

4. RESULTS

The performances of the algorithms in IQMs are given in Table 2. The highest scores are indicated with bold text and the second with the asterisk (*). The highest and second highest scores were always obtained alternately by DECUSR and RED-Net algorithms. When one of them has the highest score, the other has the second highest. According to the table, the modified DECUSR model achieved the highest scores in all metrics other than SCC for the scale 2, where RED-Net offered the highest. In PSNR measure for the scale 3, DECUSR holds the highest score. The other IQMs found the RED-Net the highest. RED-Net achieved the highest scores in all IQMs for the scale 4. VDSR yielded the third best scores in all IQMs. On the other hand, SRCNN achieved the lowest scores in all IQMs at each scale factor. Overall, the algorithms achieved remarkably high scores. For example, nearly all of the algorithms scored above 30 dB in PSNR and over 0.9 in SSIM at all scales. Even at the scale factor of two, the algorithms—E.g., DECUSR—reached 35.3151dB and 0.9553 in PSNR and SSIM respectively. In particular, the fact that the SSIM value is very close to 1.0 indicates that the success of the algorithm(s) in recovering structural finer details from LR text images. Such appealing achievements are a good indication that the algorithms can successfully produce higher resolution, and thus better quality images. Therefore, they are quite promising in TISR. To assess the algorithms in terms of human visual system, some excerpts of two predicted images by the algorithms at each scale are given in Figure 3.

The figure shows the reference image patch for two different test text images and the images of the same region predicted by the algorithms at each scale.

Figure 3. Excerpts from the predictions of the algorithms for two text images

Table 2. Scores of the algorithms for scales 2, 3 and 4

Scale	*Model*	*PSNR (dB)*	*SCC*	*SSIM*	*VIF*
	DECUSR	**35.3151**	*0.6216	**0.9553**	**0.6535**
2x	SRCNN	34.1752	0.5629	0.9391	0.5921
	VDSR	30.3865	0.5859	0.9406	0.6159
	RED-Net	*34.2038	**0.6415**	*0.9522	*0.6480
	DECUSR	**32.7401**	*0.3847	*0.9072	*0.5245
3x	SRCNN	31.2075	0.3150	0.8882	0.4777
	VDSR	32.2727	0.3799	0.9046	0.5175
	RED-Net	*32,6412	**0.3876**	**0.9094**	**0.5340**
	DECUSR	*30.7326	*0.2571	*0.8603	*0.4374
4x	SRCNN	28.7886	0.1970	0.8342	0.3862
	VDSR	30.0878	0.2549	0.8569	0.4267
	RED-Net	**31.0851**	**0.2689**	**0.8680**	**0.4574**

When examining the figure, overall, the algorithms achieved remarkably good results in recovering the details and high-frequency features. For the scale factor of two, DECUSR obtained a sharper and clearer image than the others. Besides, the text image produced by RED-Net looks similarly clear. SRCNN and VDSR, on the other hand, created aliasing especially at the edges. This aliasing effect can be seen very clearly, especially in the output images of SRCNN at higher scales. At higher scales, RED-Net produced much clearer and more successful image quality than the others, supporting the numerical results. On the other hand, DECUSR has also produced considerably good-quality text images. However, as the scale grows, TISR performance of every algorithm decreases noticeably, as expected. While a clearer image is obtained at lower scales, the images commonly become increasingly blurred as the scale increases.

In general, DECUSR produces very good text images at lower scales, whereas RED-Net provides slightly better performance at higher scales. However, the difficulties in applying RED-Net in real-world applications should be taken into account in the assessment. Because RED-Net is such a large model, it causes memory problems. Memory issues don't pose much of a problem in training, since training is accomplished by introducing very small patches of images—as is always the case—but it becomes almost impossible to run this model to process larger full-size images on GPUs, as happened in this experimental study. For this reason, all tests of this model had to be done with the computer's CPU rather than the GPU, and took days to accomplish. It is obvious that such implementation problems will make it difficult to apply algorithms to real-life problems.

In overall, the quantitative and qualitative analyses of the experiments clearly showed that the algorithms produced very promising results in the application of TISR on Ottoman archive text images.

5. CONCLUSION

The Ottoman Empire left behind a magnificent archive treasury. There are countless records and archives that can shed light on the centuries-old history of the lives, dreams and knowledge of tens of generations. It is of great importance to transfer this rich and historical heritage to the present and the future. In this context, a serious digital archive transformation and collection studies have been carried out. In particular, the quality of the digitized texts in terms of resolution will directly contribute to the success of the tasks for various purposes—e.g., text search, text analysis, and other transactions.

In this study, the resolution and quality of Ottoman archive text images were tried to be improved with SR techniques. In this context, four different models were trained to magnify text images 2, 3 and 4 times and tested both quantitatively and qualitatively. The performance of the models was found to be quite promising. This study clearly showed that SR application in archive text images will contribute positively to the processing and analysis processes of such images.

6. ABLATION STUDY

This section describes how the best hyper-parameter set was found for the modified DECUSR model. In order to find the parameter sets that maximizing the performance of DECUSR, a grid search method was performed for the following three criteria: learning rate, input image patch size, and initialization method for layer weights. The following values were taken for the learning rate: 1E-2, 1E-3 and 1E-4. For the kernel initialization, “He Normal” and “Glorot Uniform” methods were adopted. For the image sizes, the following pixel sizes were examined: 16×16, 32×32, 48×48 and 64×64 pixels. Entire values of each criteria are given in Table 3.

Table 3. Values and techniques used in the grid search for finding the best hyper parameter set. The calculation efficiency under different image patch sizes and learning rates is also an important indicator

Learning Rate	Image Patch Size	Kernel Initialization
1E-2	16×16	He Normal
1E-3	32×32	Glorot Uniform
1E-4	48×48	
	64×64	

During the grid search process, DECUSR was trained to have a maximum of 5 epochs for each of a total of 24 different parameter combinations. Afterwards, each model was tested on the test set. The top 8 models that presented the most successful performance graph—in PSNR score— were examined and the best among these was selected according to the performance value and training curve. The performance curve of the top 8 models is given in Figure 4.

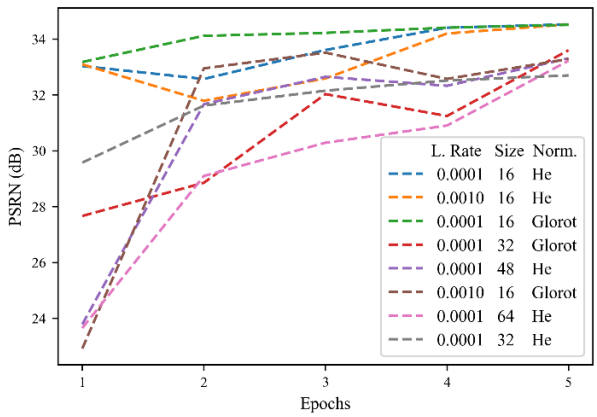

Figure 4. The top 8 training performances of DECUSR according to the three criteria: learning rate, image patch size and kernel initializer

When the characteristics of the top eight models are examined from the figure, it was observed that 7 out of 8

models and especially the first one was trained with the learning rate value of 1E-4. The top three models, and 4 out of 8 models in total, were trained with 16×16 pixel images. Additionally, the layer weights of the 5 of the 8 models and two most successful models were initialized with the "He Normal" method. So, according to the ablation study, it was concluded that the learning ability of the modified DECUSR model was best when the learning rate is 1E-4, the image size is 16×16, and the He Normal method is adopted for the kernel initialization procedure. The model was taken into comprehensive training procedure under these findings.

NOTE

This paper is the extended version of the conference paper, entitled "Towards Better Resolution of Ottoman Archive Documents" [30].

REFERENCES

[1] Rukancı, F. (2009). Arşiv Belgelerimizin Uluslararası Önemi. pp. 205-218.

[2] Yang, J., Wright, J., Huang, T., Ma, Y. (2008). Image super-resolution as sparse representation of raw image patches. In 2008 IEEE Conference on Computer Vision and Pattern Recognition, Anchorage, AK, USA, pp. 1-8. https://doi.org/10.1109/CVPR.2008.4587647

[3] Chang, H., Yeung, D.Y., Xiong, Y. (2004). Super-resolution through neighbor embedding. In Proceedings of the 2004 IEEE Computer Society Conference on Computer Vision and Pattern Recognition, 2004. CVPR 2004, Washington, DC, USA, pp. I-I. https://doi.org/10.1109/CVPR.2004.1315043

[4] Romano, Y., Isidoro, J., Milanfar, P. (2016). RAISR: rapid and accurate image super resolution. IEEE Transactions on Computational Imaging, 3(1): 110-125. https://doi.org/10.1109/TCI.2016.2629284

[5] Tang, Y., Yan, P., Yuan, Y., Li, X. (2011). Single-image super-resolution via local learning. International Journal of Machine Learning and Cybernetics, 2: 15-23. https://doi.org/10.1007/s13042-011-0011-6

[6] Dong, C., Loy, C., He, K., Tang, X. (2014). Learning a deep convolutional network for image super-resolution. In: Fleet, D., Pajdla, T., Schiele, B., Tuytelaars, T. (eds) Computer Vision – ECCV 2014. ECCV 2014. Lecture Notes in Computer Science, vol 8692. Springer, Cham. https://doi.org/10.1007/978-3-319-10593-2_13

[7] Kim, J., Lee, J.K., Lee, K.M. (2016) Accurate image super-resolution using very deep convolutional networks. IEEE Conference on Computer Vision and Pattern Recognition (CVPR), Las Vegas, NV, USA, pp. 1646-1654. https://doi.org/10.1109/CVPR.2016.182

[8] Temiz, H., Bilge, H.S. (2020). Super resolution of B-mode ultrasound images with deep learning. IEEE Access, 8: 78808-78820. https://doi.org/10.1109/ACCESS.2020.2990344

[9] Mao, X., Shen, C., Yang, Y.B. (2016). Image restoration using very deep convolutional encoder-decoder networks with symmetric skip connections. Advances in Neural Information Processing Systems, 29.

[10] Sevinç, Ö., Mehrubeoglu, M., Güzel, M., Askerzade, I. (2022). An effective medical image classification: Transfer learning enhanced by auto encoder and classified with SVM. Traitement du Signal, 39(1): 125-131. https://doi.org/10.18280/ts.390112

[11] Wajeed, M.A., Sreenivasulu, V. (2019). Image based tumor cells identification using convolutional neural network and auto encoders. Traitement du Signal, 36(5): 445-453. https://doi.org/10.18280/ts.360510

[12] Ledig, C., Theis, L., Huszár, F., Caballero, J., Cunningham, A., Acosta, A., Aitken, A., Tejani, A., Totz, J., Wang, Z., Shi, W. (2017). Photo-realistic single image super-resolution using a generative adversarial network. In Proceedings of the IEEE conference on computer vision and pattern recognition, Honolulu, HI, USA, pp. 4681-4690. https://doi.org/10.1109/CVPR.2017.19

[13] Zareapoor, M., Celebi, M.E., Yang, J. (2019). Diverse adversarial network for image super-resolution. Signal Processing: Image Communication, 74: 191-200. https://doi.org/10.1016/j.image.2019.02.008

[14] Wu, F., Wang, B., Cui, D., Li, L. (2018). Single image super-resolution based on Wasserstein GANs. In 2018 37th Chinese Control Conference (CCC), Wuhan, China, pp. 9649-9653. https://doi.org/10.23919/ChiCC.2018.8484039

[15] Zhu, X., Zhang, L., Zhang, L., Liu, X., Shen, Y., Zhao, S. (2019). Generative adversarial network-based image super-resolution with a novel quality loss. In 2019 International Symposium on Intelligent Signal Processing and Communication Systems (ISPACS), Taipei, Taiwan, pp. 1-2. https://doi.org/10.1109/ISPACS48206.2019.8986250

[16] Wang, Z., Chen, J., Hoi, S.C. (2020). Deep learning for image super-resolution: A survey. IEEE Transactions on Pattern Analysis and Machine Intelligence, 43(10): 3365-3387. https://doi.org/10.1109/TPAMI.2020.2982166

[17] Anwar, S., Khan, S., Barnes, N. (2020). A deep journey into super-resolution: A survey. ACM Computing Surveys (CSUR), 53(3): 1-34. https://doi.org/10.1145/3390462

[18] Nayef, N., Chazalon, J., Gomez-Krämer, P., Ogier, J.M. (2014). Efficient example-based super-resolution of single text images based on selective patch processing. In 2014 11th IAPR International Workshop on Document Analysis Systems, Tours, France, pp. 227-231. https://doi.org/10.1109/DAS.2014.25

[19] Banerjee, J., Jawahar, C.V. (2008). Super-resolution of text images using edge-directed tangent field. In 2008 The Eighth IAPR International Workshop on Document Analysis Systems, Nara, Japan, pp. 76-83. https://doi.org/10.1109/DAS.2008.26

[20] Dalley, G., Freeman, B., Marks, J. (2004). Single-frame text super-resolution: A Bayesian approach. In 2004 International Conference on Image Processing, 2004. ICIP'04, vol. 5, Singapore, pp. 3295-3298. https://doi.org/10.1109/ICIP.2004.1421818

[21] Sattar, F., Tay, D.B. (1999). Enhancement of document images using multiresolution and fuzzy logic techniques. IEEE Signal Processing Letters, 6(10): 249-252. https://doi.org/10.1109/97.789601

[22] Fu, Z., Kong, Y., Zheng, Y., Ye, H., Hu, W., Yang, J., He, L. (2019). Cascaded detail-preserving networks for super-resolution of document images. In 2019 International Conference on Document Analysis and Recognition (ICDAR), Sydney, NSW, Australia, pp.

240-245. https://doi.org/10.1109/ICDAR.2019.00047
[23] Su, X., Xu, H., Kang, Y., Hao, X., Gao, G., Zhang, Y. (2019). Improving text image resolution using a deep generative adversarial network for optical character recognition. In 2019 International Conference on Document Analysis and Recognition (ICDAR), Sydney, NSW, Australia, pp. 1193-1199. https://doi.org/10.1109/ICDAR.2019.00193
[24] Peng, X., Wang, C. (2020). Building super-resolution image generator for OCR accuracy improvement. In: Bai, X., Karatzas, D., Lopresti, D. (eds) Document Analysis Systems. DAS 2020. Lecture Notes in Computer Science(), vol 12116. Springer, Cham. https://doi.org/10.1007/978-3-030-57058-3_11
[25] Peyrard, C., Baccouche, M., Mamalet, F., Garcia, C. (2015, August). ICDAR2015 competition on text image super-resolution. In 2015 13th International Conference on Document Analysis and Recognition (ICDAR), Tunis, Tunisia, pp. 1201-1205. https://doi.org/10.1109/ICDAR.2015.7333951
[26] Kodym, O., Hradiš, M. (2022). TG^2: Text-guided transformer GAN for restoring document readability and perceived quality. International Journal on Document Analysis and Recognition (IJDAR), 25(1): 15-28. https://doi.org/10.1007/s10032-021-00387-z
[27] Ronneberger, O., Fischer, P., Brox, T. (2015). U-net: Convolutional networks for biomedical image segmentation. In: Navab, N., Hornegger, J., Wells, W., Frangi, A. (eds) Medical Image Computing and Computer-Assisted Intervention – MICCAI 2015. MICCAI 2015. Lecture Notes in Computer Science(), vol 9351. Springer, Cham. https://doi.org/10.1007/978-3-319-24574-4_28
[28] Nguyen, K.C., Nguyen, C.T., Hotta, S., Nakagawa, M. (2019). A character attention generative adversarial network for degraded historical document restoration. In 2019 International Conference on Document Analysis and Recognition (ICDAR), Sydney, NSW, Australia, pp. 420-425. https://doi.org/10.1109/ICDAR.2019.00074
[29] Uzun, A., Özer, A., Turkmen, H.I. (2021). Evrişimsel Sinir Ağı Tabanlı Osmanlıca Belge Çözümleyici. International Journal of Advances in Engineering and Pure Sciences, 33(4): 581-591. https://doi.org/10.7240/jeps.888164
[30] Temiz, H. (2023). Towards better resolution of ottoman archive documents. 3rd International Conference on Engineering and Applied Natural Sciences, Konya, Turkiye, pp. 564-568. https://drive.google.com/file/d/1kWX2SHgA_Y9_ZSuLEBtB0ETGtW5-6QHM/view.
[31] Wikilala. https://www.wikilala.com, accessed on Mar. 02, 2022.
[32] Muteferriqa. https://muteferriqa.com, accessed on Nov. 02, 2022.
[33] Department of State Archives, https://katalog.devletarsivleri.gov.tr, accessed on Nov 01, 2022.
[34] Temiz, H. (2023). DeepSR: A deep learning tool for image super resolution. SoftwareX, 21: 101261. https://doi.org/10.1016/j.softx.2022.101261
[35] Wang, Z., Bovik, A.C., Sheikh, H.R., Simoncelli, E.P. (2004). Image quality assessment: from error visibility to structural similarity. IEEE Transactions on Image Processing, 13(4): 600-612. https://doi.org/10.1109/TIP.2003.819861
[36] Zhou, J., Civco, D.L., Silander, J.A. (1998). A wavelet transform method to merge Landsat TM and SPOT panchromatic data. International journal of remote sensing, 19(4): 743-757. https://doi.org/10.1080/014311698215973
[37] Alparone, L., Aiazzi, B., Baronti, S., Garzelli, A., Nencini, F., Selva, M. (2008). Multispectral and panchromatic data fusion assessment without reference. Photogrammetric Engineering & Remote Sensing, 74(2): 193-200.
[38] Deshpande, R.G., Ragha, L.L., Sharma, S.K. (2018). Video quality assessment through PSNR estimation for different compression standards. Indonesian Journal of Electrical Engineering and Computer Science, 11(3): 918-924. https://doi.org/10.11591/ijeecs.v11.i3.pp918-924